Nanoscale

Electrospun Nanofiber Mat as an Electrode for AC-Dielectrophoretic Trapping of Nanoparticles

Journal:	*Nanoscale*
Manuscript ID	NR-COM-09-2023-004496.R1
Article Type:	Communication
Date Submitted by the Author:	02-Nov-2023
Complete List of Authors:	Mondal, Tonoy Kumar; University of Louisville, Mechanical Engineering West, Jacob; University of Louisville, Mechanical Engineering Williams, Stuart; University of Louisville, Mechanical Engineering

Electrospun Nanofiber Mat as an Electrode for AC-Dielectrophoretic Trapping of Nanoparticles

*Tonoy K. Mondal, J. Hunter West, Stuart J. Williams**

Department of Mechanical Engineering, University of Louisville, Louisville, KY-40292, USA

***Corresponding Author: stuart.williams@louisville.edu**

KEYWORDs

Dielectrophoresis, electrokinetics, micro/nanoparticles, colloids, electrospinning, nanofibers, electrohydrodynamics

ABSTRACT

In order to trap nanoparticles with dielectrophoresis, high electric field gradients are needed. Here we created large area (> mm^2) conductive carbon nanofiber mats to trap nanoparticles with dielectrophoresis. The electrospun fiber mats had an average diameter of 267±94 nm and a conductivity of 2.55 S/cm. Relative to cleanroom procedures, this procedure is less expensive in creating bulk conductive nanoscale features. The electrospun fiber mat was used as one electrode, with an indium-tin-oxide glass slide serving as the other (separated approximately 150 µm). Numerical models showed that conductive nanoscale fibers can generate significant field gradients sufficient to overcome Brownian transport of nanoparticles. Our experiments trapped 20 nm fluorescent polystyrene beads at 7 V_{rms} and 1 kHz. Trapping is further enhanced through simultaneous electrohydrodynamic motion. Overall, this straightforward electrospun fiber mat can serve as a foundation for future use in microscale electrokinetic devices.

Body Text

It is crucial to capture, translate, and assemble nanoparticles in order to effectively characterize materials and achieve self/controlled assembly of nanoscale objects[1, 2]. There are various methods for assembling and concentrating nanoparticles, such as optical[3], thermal[4], electrostatic[5], and electrokinetic[6-8] techniques. As target particles become smaller, much greater input power is needed for effective trapping as many of these forces scale with the volume of the particle. Often there are physical and/or equipment limitations in applying larger inputs (for example, larger voltages could induce electrolysis). In many cases, forces are enhanced by incorporating nanoscale features that concentrate such forces. However, building these nanoscale features using micro- and nanofabrication techniques, especially over a relatively larger area, could be costly and necessitate a cleanroom for fabrication [9, 10]. This manuscript shows a relatively low cost method of creating conductive nanofibers (CNF) whose nanoscale features inherently enhance electrokinetic effects. This is demonstrated herein by demonstrating the trapping of nanoparticles with a combination of dielectrophoresis (DEP) and electrohydrodynamic flow. Numerical simulations show that these electrokinetic effects are significant for sub-micrometer fibers. Next and introduction to CNF is discussed followed by an introduction to DEP and challenges associated with trapping nanoparticles. To our knowledge, this is the first study to demonstrate DEP trapping of particles using CNF and, thus, illustrates the first step towards high-throughput DEP-enhanced trapping of nanoparticles.

Carbon nanofibers (CNF), whose diameters are less than 1 μm, can be created by electrospinning. Electrospinning is a relatively simple system, it employs electrostatic forces created by high voltage applied between a syringe needle and a collector. A liquid jet is formed when the electrostatic forces overcome surface tension, resulting in the polymer solution being pulled to the collector, creating a thin, non-woven fiber mat which is submicron in diameter[11-14]. CNFs are a highly promising material with a wide range of potential applications, including nanoelectronics, electrode materials, energy storage devices and fillers in nanocomposite materials [15-19]. Using electrospinning, it is possible to create conductive nanofiber mats by stabilizing and then carbonizing polyacrylonitrile, which is commonly used as a precursor for CNFs [20], lignin fibers [21], and other nanofiber mats. The polymers' conductivity can be enhanced by incorporating additional conductive carbon elements like carbon nanotubes (CNT) [22, 23], graphite [24], and carbon black [25]. Among them, CNTs of various types are widely employed since the addition of a tiny amount (< 5% wt) improves mechanical qualities, thermal stability and electrical conductivities [26, 27]. However, the poor dispersion of these other components into the CNFs is one challenge integrating these compounds as fillers [28]. The most frequently used

technique for dispersing CNTs involves ultrasonication of the CNTs in solvents [29] and/or addition of other chemical components to ensure a uniform distribution [26].

Although nanofiber mats have been extensively used for filtration [30], to our knowledge CNF mats have not been used as an electrode to enhance particle trapping. In order to understand how CNFs enhance electrokinetic trapping, an introduction to dielectrophoresis (DEP) is needed. DEP is an electrokinetic motion that uses the interaction between a non-uniform electric field and an induced dipole to manipulate liquid suspended particles [31]. Particles can be attracted to high field gradients (positive DEP or pDEP) or repelled from them (negative DEP or nDEP), depending on their net polarization. The Clausius-Mossotti factor will determine the AC frequency response of the spherical particles and the DEP direction and is given by [32]:

$$CM(\omega) = \frac{\tilde{\varepsilon_p} - \tilde{\varepsilon_m}}{\tilde{\varepsilon_p} + 2\tilde{\varepsilon_m}}, \text{ where } \tilde{\varepsilon} = \varepsilon - j\frac{\sigma}{\omega} \quad (1)$$

where complex permittivity is $\tilde{\varepsilon}$(*m* and *p* are medium and particle, respectively), angular frequency is ω ($\omega = 2\pi f$), conductivity is σ, and *j* is $\sqrt{-1}$. For a spherical particle with radius *a*, and applied electric field *E*, the time average DEP force can be expressed as

$$< \vec{F}_{DEP} >= 2\pi\varepsilon_m a^3 \mathrm{Re}(CM)\nabla|E|^2 \quad (2)$$

where, $\mathrm{Re}(CM)$ is the real part of the Clausius-Mossotti factor. Based on Equation 2, generating a large electric field gradient is one method of increasing the DEP force. This can be achieved by various ways of designing and/or optimizing tiny geometries in microfluidics devices, i.e. electrokinetic nanoprobes,[33] micro/nano gap electrodes,[34, 35] nanowire electrodes,[36] metal tips,[37] etc. Researchers have also used carbon-based micro/nanoscale materials such as carbon nanotubes [38-40] and carbon nanofibers[41, 42] to generate high field gradients and demonstrated trapping and manipulating nanoparticles and bio-particles such as DNA. In the literature, there have been reports of using porous micro-fabricated features to trap particulates using DEP. In such studies, typically these features incorporate insulator-based DEP trapping[43, 44]. Some researchers have also used high surface area fabrics in insulator-based devices to trap larger micro-particles[45]. Unfortunately, these studies did not demonstrate nanoparticle trapping as their geometries are approximately on the microscale and thus cannot generate sufficient DEP forces.

In the studies mentioned, conductive features were created by either using metal electrodes patterned using traditional fabrication techniques or by growing carbon-based materials through chemical vapor deposition. Additionally, the geometries used were either single features or of limited surface area, thereby limiting bulk particle trapping. By examining these studies, there is a clear gap in using nanoporous material with a larger surface area as a direct electrode and trapping bulk nanoparticles instead of larger microparticles. This study demonstrates the use of electrospun conductive nanofiber mat to serve as an electrode for DEP trapping of nanoparticles. The following shows successful trapping of 1.0 µm, 210 nm and 20 nm fluorescence polystyrene particles using a CNF electrode mat. Further, our simulations show that using an array of fibers produces an electric

field gradient strong enough to overcome Brownian motion and trap particles by DEP. This simple method of nanofiber fabrication does not require cleanroom fabrication and can be deposited over large areas (> cm^2). This could potentially serve as a new electrode in DEP devices in future research.

When a sub-micrometer particle is subjected to a force, its resulting velocity can be interpreted as moving at its terminal velocity [46, 47]; this is because the inertial time scale of micro- and nanoparticles is usually insignificant. Therefore, when an external force is applied to such particles they can be considered to move at terminal velocity as their characteristic time of acceleration is on the order of 10^{-6} s [48]. For our case, the terminal velocity of a spherical particle under an applied DEP force is

$$v_{DEP} = F_{DEP}/6\pi\eta a \quad (3)$$

where η is fluid viscosity. Particles are also simultaneously experiencing Brownian motion. We refer to the RMS Brownian displacement of a particle in one second as its effective Brownian motion velocity, defined by

$$v_B = \sqrt{\frac{k_B T}{3\pi\eta a}} \quad (4)$$

where, temperature is *T* and k_B is Boltzmann's constant. To trap particles using DEP, this velocity in Equation (4) serves as threshold velocity. In other words, the AC electric field needs to be applied such that $v_{DEP} > v_B$ in order to meet our trapping criteria. If we set these two velocities equal, we can solve for a desired minimum gradient of field-squared ($\nabla|E|^2$). Table 1 shows the resulting gradient of field-squared when *T* = 298 K and Re*(CM)* = 1.0 for the particles in this study. Using this approach, the required field gradient for any spherical particle would be

$$\nabla E^2 = 0.002708 a^{-2.5} \quad (5)$$

Table 1: Required gradient of field square for trapping of different sized particles when considering random Brownian displacements only.

Particle diameter (2*a*, nm)	Required gradient field squared (V^2/m^3)
20	2.71×10^{17}
210	7.58×10^{14}
1000	1.53×10^{13}

For example, 20 nm particles require 357.5 times greater gradient of field-squared compared to 210 nm particles. To put this into perspective, consider a DEP system whose electrode geometry is fixed (i.e., field non-uniformities are defined). The DEP force is proportional to voltage squared and, in order to have $\nabla|E|^2$ increase by 357.5, the voltage would need to increase by a factor of 18.9. Unfortunately, this significant increase in voltage is not feasible in some DEP systems due to constraints on waveform generators, the presence of electrolysis, and the temperature increase due to joule heating[33]as these compromise the experiment. Therefore, we believe that the use of conductive nanofibers as can significantly increase the gradient of field-squared due to their inherent geometrical properties.

Our CNF recipe is a variation of Peter, et al. [26] and is illustrated in Figure 1. First, multi-walled carbon nanotubes (MWCNTs, 30-50 nm OD from Cheap Tubes Inc.) were suspended in N, N-Dimethylformamide (anhydrous, 99.8% from Sigma Aldrich) and ultrasonicated for about 5 hours to ensure that the tubes were completely dispersed. Next, polyacrylonitrile (M_w=150,000 from Sigma Aldrich) and phthalic acid (ACS reagents, ≥ 99.5% from Sigma Aldrich) were added and stirred for 2 hours at 60 ℃ (Figure 1a). The solution was transferred to a syringe with a blunt needle of size 22G for electrospinning. The flow rate was 0.5 mL/h, voltage was 12 kV DC, 10 cm collector gap, and 25-30% relative humidity (Figure 1b). Once collected, the fibers were stabilized (in atmosphere) and carbonized (in N_2 atmosphere) (Figure 1c). The CNF mat was imaged using Apreo scanning electron microscope (SEM) to characterize the carbonized fibers, observing their morphology and diameter distribution (refer to Figure S1). The final CNF mat had an average diameter of 267± 94 nm (measured using ImageJ for 100 measurements). Mat conductivity was measured using four-point probe measurements, which was 2.55 S/cm for an 80 µm thick CNF mat (Figure 1d). More details of the electrospinning process can be found in Supporting Information.

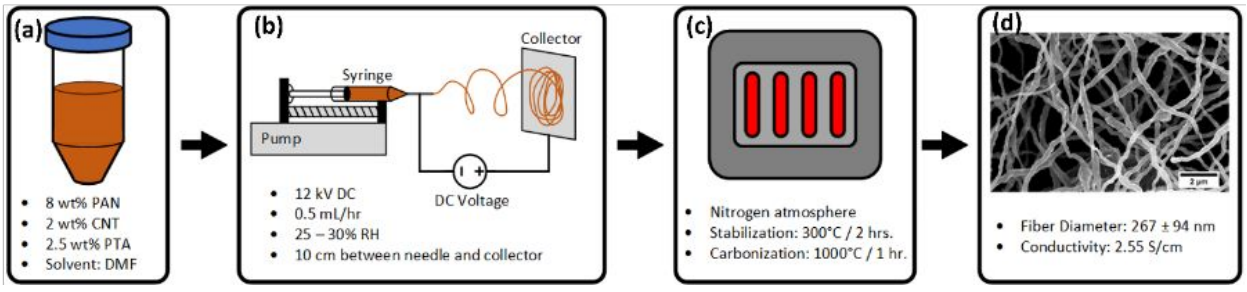

Figure 1. Process flow diagram of electrospinning: (a) details of the recipe and materials used; (b) schematic of an electrospinning setup with process parameters used; (c) carbonization process and temperature used to heat treat the mat; (d) SEM image of the mat, average diameter (measured from SEM images) and conductivity (four-point-probe) of the mat.

To determine the impact of our conductive fibers on the gradient of field-squared, we conducted 2D numerical simulations (COMSOL Multiphysics) of an array of conductive fibers (Figure 2). Details of the simulation space and boundary conditions can be found in the Supporting Information (Figure S2a). In brief, the Laplace equation is used to determine the electric field, which can be expressed mathematically as[49]

$$\nabla^2\varphi = 0 \tag{6}$$

where, φ denotes the applied electric potential to the electrodes. Next, the electric field strength $\vec{E}$ can be determined as

$$\vec{E} = -\nabla\varphi \tag{7}$$

The gradient of field-squared is then calculated form the simulated field. Our simulation had 7 V_{rms} applied across the fibers with a diameter of 250 nm and a plate spaced 150 µm apart (Figure 2a); these dimensions are approximately the same as our experiment (discussed later). The objective of the model was to verify that our fibers could produce sufficient electric field gradients to trap nanoparticles and meet the thresholds in Table 1. Although our experimental mat does not have fibers geometrically ordered nor aligned, we believe that the triangular arrangement within the simulation provides an appropriate estimation of the electric field gradient in the vicinity of the fibers. Based on SEM image analysis, the average pore size was estimated to be 1.5 µm and this value was used as spacing between fibers in the numerical simulation.

The maximum $\nabla|E|^2$ was 2.82×10^{17} V^2/m^3 around the fiber edges (Figures 2a and 2b) and is theoretically sufficient for trapping 20 nm (see Table 1). From Figure 2c, the $\nabla|E|^2$ increases as it approaches the fiber and, thus, there is an effective trapping region around the fiber depending on the required threshold. The electrode gap could be reduced and/or the applied voltage increased (> 7 V_{rms}) to increase DEP forces. Nonetheless, the generated gradient is sufficient not only for trapping 20 nm particles but also comparable to other studies that used more complex nanoscale fabrication schemes [8, 36].

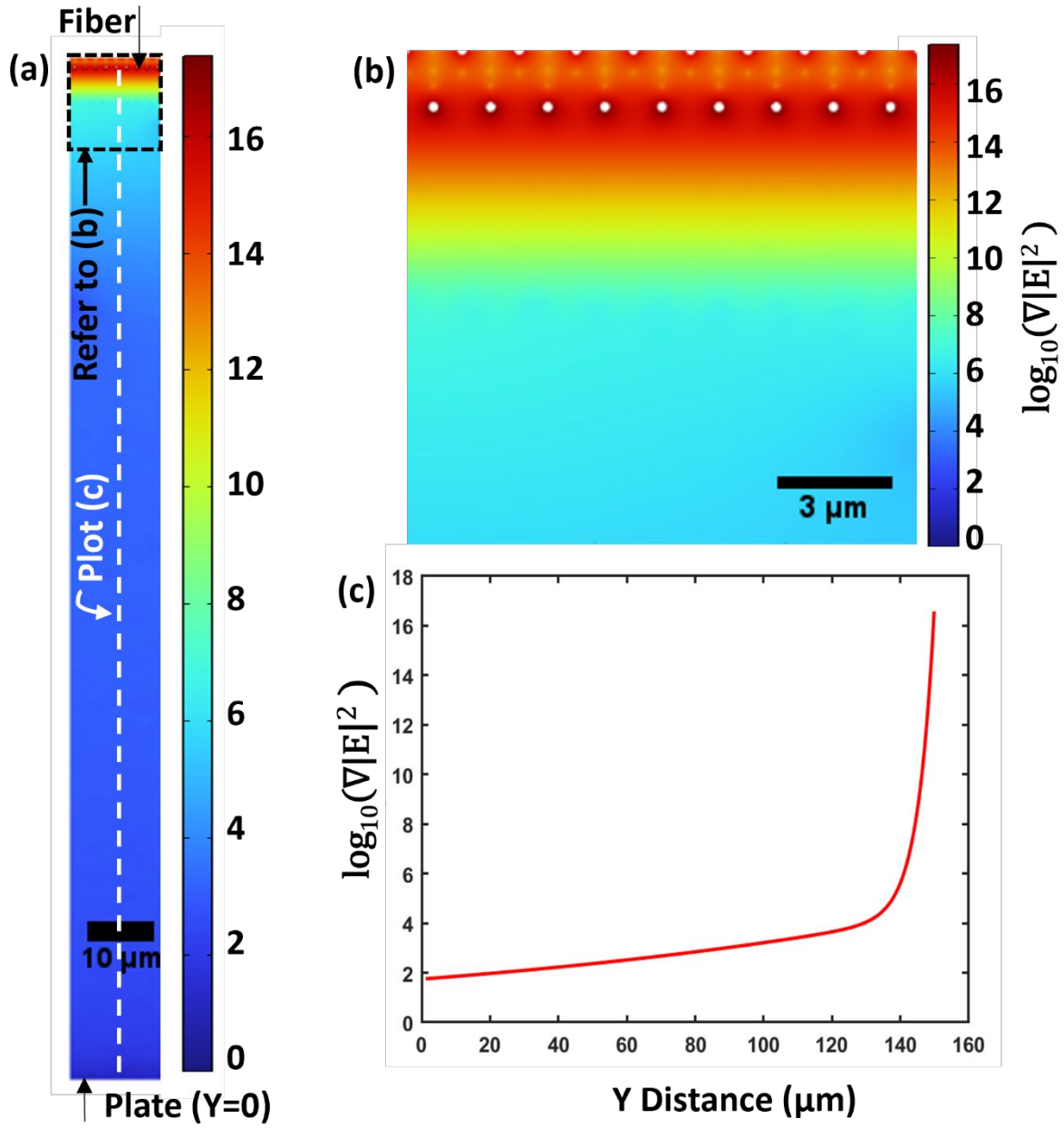

Figure 2. Finite-element method simulations of an array of 250 nm diameter fibers and an ITO plate with 150 µm spacing. (a) The resulting gradient of the electric field squared (log scale) when 7 V_{rms} is applied. The highest magnitude of $\nabla|E|^2$ found near the fiber edges is approximately 2.82×10^{17} V^2/m^3. (b) Zoomed in view of $\nabla|E|^2$ near the fiber edge. (c) Plot of $\nabla|E|^2$ from the plate (*Y* = 0 µm) to the fiber (*Y* = 150 µm). The electric potential distribution is included in the Supporting Information Figure S2b.

Two sets of additional simulations were conducted to gain more insights on the gradient of field-squared generated by the nanofibers. In the first set of simulations, the center-to-center spacing between the fibers changed from 0.5 μm to 20 μm while keeping the fiber radius fixed at 0.125 μm. The contour of the gradient of field-squared (log scale) is shown in Figures 3a and 3b for a spacing of 1 μm and 10 μm, respectively. The generated gradient of field-squared along the axis labeled in Figure 3a for all simulated values is shown in Figure 3e. In the second set of simulations, the fiber radius was varied from 0.05 μm (Figure 3c) to 2.5 μm (Figure 3d) with fixed spacing between two fibers (1.5 μm). Figure 3f shows the gradient of field-squared for this set of simulations along the axis labeled in Figure 3a. From Figure 3e, increasing fiber spacing led to an increase in the spatial range of the high gradients away from the fiber mat. Intuitively, this means that more spacious regions are more likely to draw in particles from the bulk via DEP if the gradient of field-squared meets certain thresholds as mentioned in Table 1. However, if you compare the gradient of field-squared in the area between adjacent fibers, larger spacing decreases the DEP force in this region. Thus, there are voids between adjacent fibers that may have insufficient DEP forces to trap particles. Similarly, if the fiber radius increased with a fixed pore size (Figure 3c and 3d), the strength adjacent to the fiber surface decreased but the spatial range increased (Figure 3f). The simulated maximum gradient of field-squared for different fiber radii is shown in Table 2. From these simulations, smaller fiber diameters produce greater local values of the gradient of field-squared, but smaller pore sizes limit their spatial range.

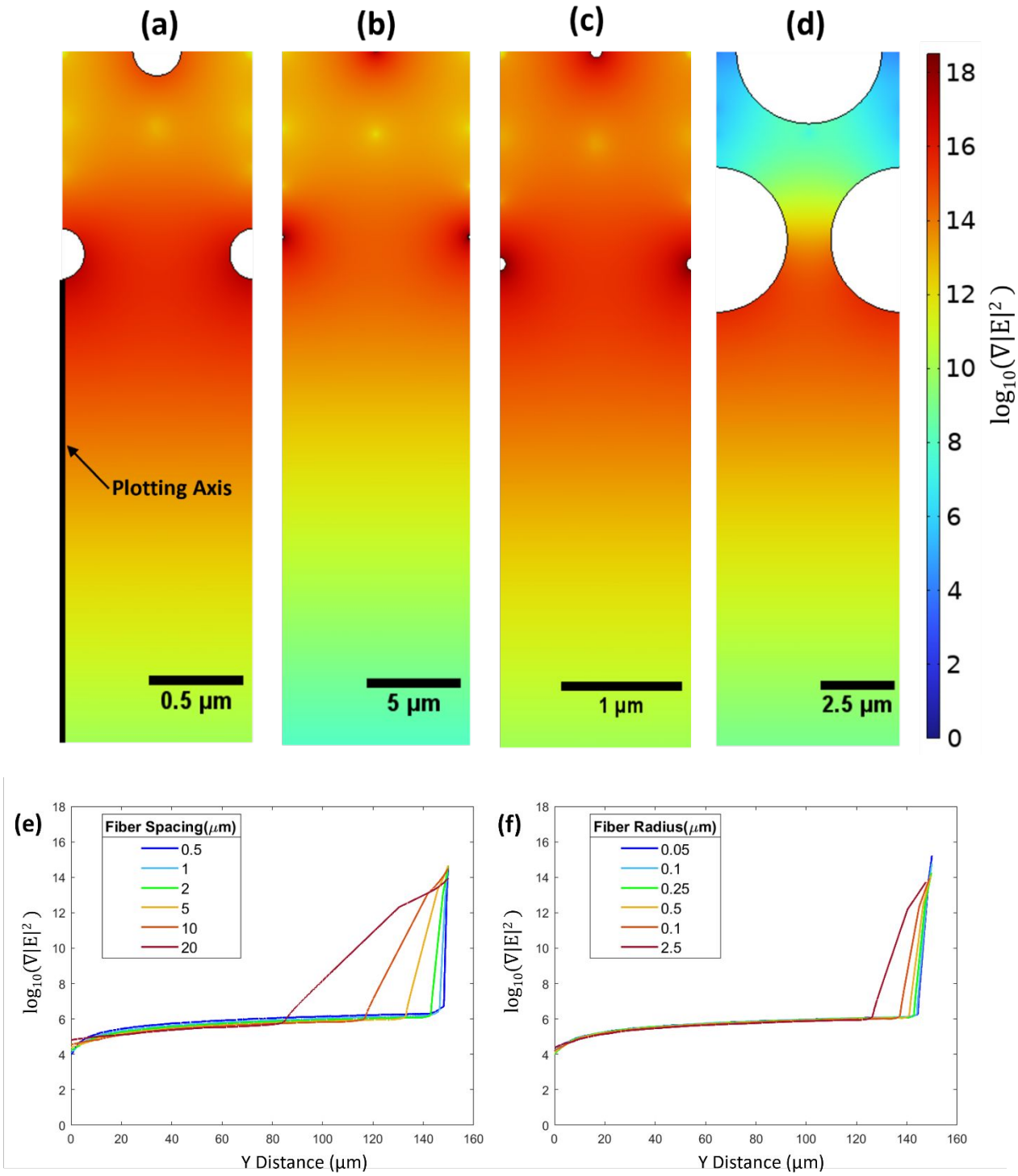

Figure 3. The gradient of field-squared for (a) fiber radius of 0.125 μm and 1 μm spacing, (b) fiber radius of 0.125 μm and 10 μm spacing, (c) fiber radius of 0.05 μm and 1.5 μm spacing, and (d) fiber radius 2.5 μm and 1.5 μm spacing. Note different length

scale bars. Plot of $\nabla|E|^2$ along the axis indicated in (a) for (e) constant fiber radius and varying spacing, and (f) constant spacing and varying fiber radius.

Table 2. Maximum electric field gradient-squared produced for different fiber radius using numerical simulations by keeping pore space constant (1.5 μm).

Fiber radius (nm)	Maximum gradient field squared (V^2/m^3)
50	2.51×10^{18}
100	5.01×10^{17}
250	7.94×10^{16}
500	3.16×10^{16}
1000	1.12×10^{16}
2500	3.89×10^{15}

The DEP experiments were carried out using an inverted fluorescent microscope (Nikon Eclipse Ti-U) and a 20X objective lens, as depicted in Figure 4. An ITO-coated glass slide (8-12 Ω, SPI supplies) was used as a planar electrode and enabled observation of the CNF mat. A circular silicon well, approximately 15 mm in diameter, was adhered to the ITO to contain the particle solutions. Another electrode was created using a strip of CNF mat (approximately 80 μm thick and 3 mm wide) sandwiched between copper tape. The CNF mat probe was fixed to a micromanipulator that adjusted the mat electrode height until it had a spacing of about 150 μm above the ITO electrode. An AC signal was applied to the electrodes with a benchtop arbitrary waveform generator (Keithley 3390). Real-time monitoring of particle movement, as well as capturing images before and after the experiment, was done using a cooled CCD camera (PCO Sensicam QE).

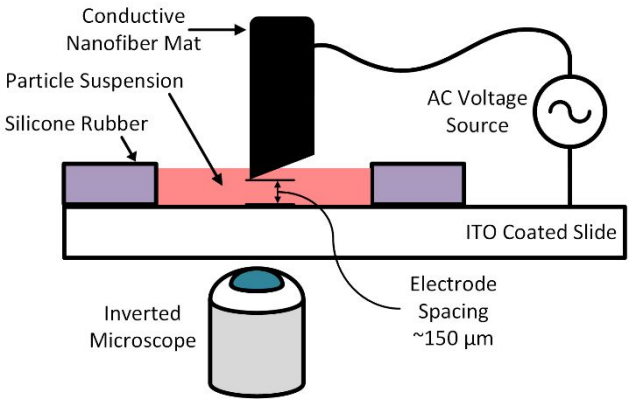

Figure 4. Illustration of experimental setup used for DEP concentration of nanoparticles.

We used three types of fluorescent nanoparticle polystyrene suspensions, 210 nm and 1.0 μm red fluorescent particles (initially 1% solids, Fluro-Max) and 20 nm carboxylate-modified red fluorescent particles (2% solids, Invitrogen). To prepare the trapping solution, we added approximately two drops (20 μL) of particle solution to 5 mL of DI water (filtered from Milli-Q ultrapure water system) with 0.1% Tween 20 (Thermo-Scientific). The final solution had a medium conductivity of $\sigma_m = 3.08 \times 10^{-3} S/m$, as measured by Denver Instrument Model 220 conductivity meter. Next, 400 μL of DI water/Tween solution was added to the well to allow presoaking of the CNF mat. Then 100 μL of particle solution was added to the well before an electric field was applied. The resulting particle concentrations were approximately 15×10^6 1.0 μm particles/mL, 1.6×10^9 210 nm particles/mL, and 3.6×10^{12} 20 nm particles/mL.

Figure 5 shows the results of DEP trapping using a CNF mat electrode. For these experiments, we applied an electric potential of 7 V_{rms}, 1 kHz between the CNF mat electrode and the ITO electrode. First, images were acquired before the application of the applied field, which was applied for approximately two and a half minutes before an image was acquired (Figure 5). We observed bulk particle trapping on the nanofiber mat surfaces for all three particles. Trapped fluorescent particles are shown with the brighter regions (Figure 5b, 5e, 5g). Most of the trapping occurred at the perimeter of the cut mat where it was closest to the ITO electrode. Also, we observed significant electrohydrodynamic fluid motion which likely enhanced DEP trapping. For better depiction of particle trapping, we have included a time-lapse series of images with 20 nm particles in Supplementary Information (Figure S3). Next, we removed the CNF mat from the solution and allowed it to dry at room temperature. We then imaged the mat under SEM to view the individual trapped particles. The SEM images of trapped 1.0 μm particles are shown in Figure 5c and in Figure 5h for 210 nm particles.

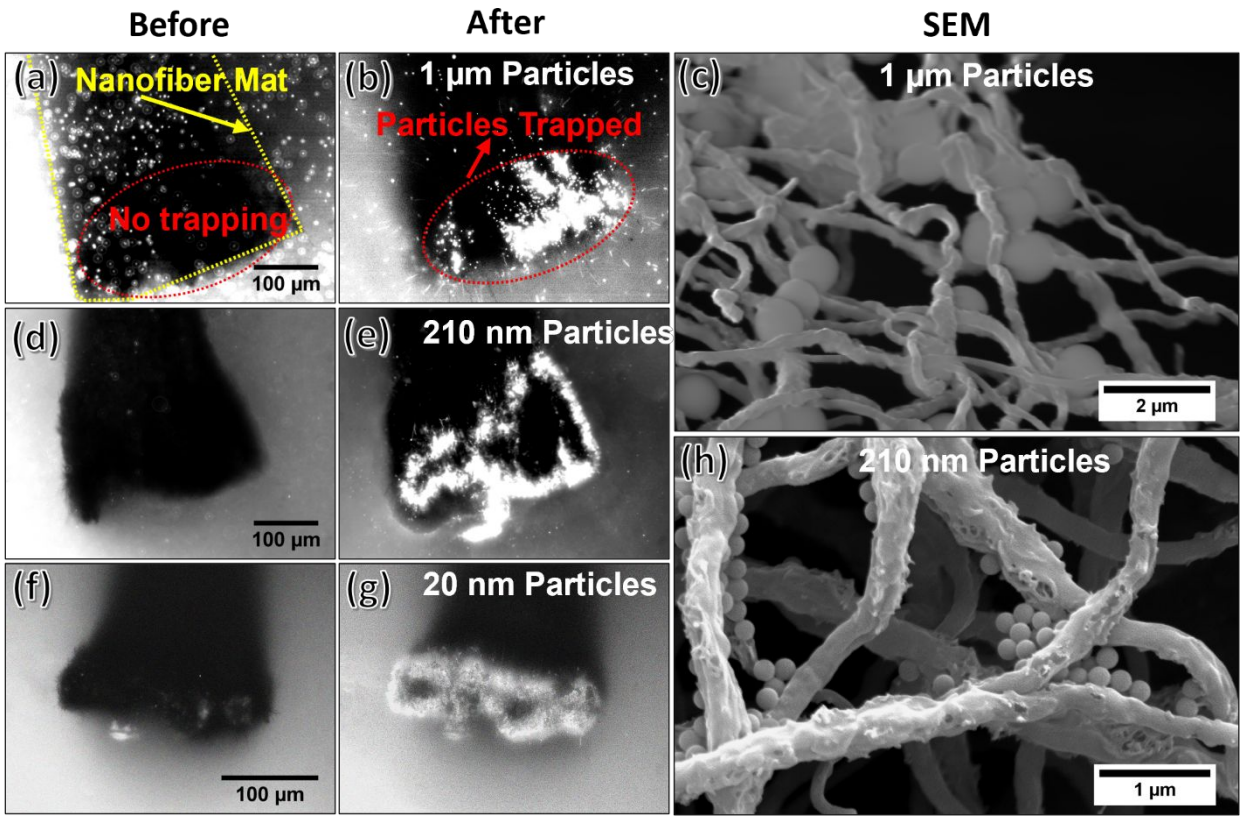

Figure 5. Experimental image set acquired from fluorescence microscope as well as scanning electron microscope. Experiment with 1.0 µm particles (a) before and (b) after the applied AC field and (c) its SEM image after drying. Experiment with 210 nm particles (d) before and (e) after the applied AC field and (h) its SEM image after drying. Experiment with 20 nm particles (f) before and (g) after the applied AC field. Scale bars are placed on the left side of the fluorescence image as their corresponding right has same scaled bar. SEM images have their own scale bar. The field was applied approximately 150 sec.

Experiments were repeated with 1.0 µm particles at a range of frequencies (1 kHz to 1 MHz) at 7 V_{rms} in order to better visualize the AC frequency dependence of our system. The expected frequency dependence of Re(*CM*) is shown in Supporting Information (Figure S2c) for 1.0 µm polystyrene particles ($\sigma_p = 4\ mS/m$ and $\mathcal{E}_p$=2.25$\mathcal{E}_0$ with $\mathcal{E}_0$ is $8.85 \times 10^{-12}\ F/m$) with the crossover frequency (Re(*CM*)=0) calculated to be 520 kHz. Thus, at lower frequencies, we expected the particles to be attracted (pDEP) towards the CNF mat electrode and repelled at higher frequencies (nDEP). The Supplementary Information video shows the observed frequency behavior of this system. In the video, the frequency starts at 1 kHz and is increased in discrete steps until 1 MHz. Particle attraction was observed until the frequency reached 500 kHz. At higher frequencies particle movements decreased and we observed little or no movement. At 1 MHz, particles experienced strong repulsion and moved away from the fiber mat

electrode (though some trapped particles remained stuck). These frequency dependent observations are in alignment with our crossover frequency calculations.

During experiments we observed a long-range circulation of the fluid and particles were attracted from further distances than anticipated. The simulation effectively demonstrated that the DEP is not a long-range attraction as the gradient of field squared is relatively low until it gets close to the fiber surface (Figure 2c). Additionally, from Figure S1a, there is roughness on the fiber surfaces and that may cause local gradients a bit higher than what the simulation predicted. This led us to believe that electrohydrodynamic mechanisms coupled with DEP forces enhance long-range particle trapping. The applied AC field may induce electrothermal flow and/or AC electro-osmosis [49]. This fluid circulation would enhance DEP trapping by translating particles from the bulk into trapping regions close to the fiber. Due to our low conductivity media, both electrothermal and AC electro-osmotic flows may be present [46, 49]. In order to assess electrothermal flow further, its relaxation is typically associated with the charge relaxation frequency of the electrolyte is calculated[50] $\sigma_m/2\pi\mathcal{E}_m$ = 710 kHz. Electrothermal flows are generally stronger at frequencies less than the relaxation frequency compared to higher frequencies (see Supplemental Information for a description of the electrothermal flow body force). Although electrothermal flow around individual fibers was not visualized within this study, the expected flow patterns for both frequency regimes in illustrated in Supplemental Figure S4. AC electro-osmosis also decreases at increasing AC frequencies[51]. The slower particle motion observed at higher frequencies (Supplemental Movie) is consistent with these characteristics. For experiments conducted at 1 kHz (Figure 5), the presence of AC electro-osmotic flow is highly likely due to the use of low conductivity fluid (3.08 mS/m). Additional experimentation is needed using fluids of different conductivities to assess the impact of AC electrohydrodynamics on CNF DEP trapping.

Conclusions

To summarize, we have shown that bulk electrokinetic nanoparticles trapping can be achieved using an electrode made from an electrospun nanofiber mat. Trapping was due to both dielectrophoresis and electrohydrodynamics. The implementation and use of conductive nanofibers adds a new dimension to electrokinetic microfluidic devices. Electrospinning and similar nanofiber fabrication procedures enables a straightforward method of creating large area (> cm^2) conductive nanofibers that inherently have significant field gradients. Our proof-of-concept DEP nanofiber system successfully trapped nanoparticles as small as 20 nm in diameter and, in theory, has sufficient forces to trap proteins[52]. This study provides a foundation for further nanofiber-based systems, which complements the decades-long history of electrospinning. In addition, we envision DEP-enhanced high throughput filtration systems to process liquid volumes at a rate significantly higher than current DEP systems with throughput limitation [53].

Supporting Information

Figure showing the SEM image of the heat-treated CNF mat (Figure S1a). Histogram showing the diameter distribution of the heat-treated CNF mat with normal distribution curve (Figure S1b). Modeling schematic for an array of fibers and plate configuration (Figure S2a). The electric potential distribution when 7 V_{rms} is applied within the modeling domain (Figure S2b). Re(*CM*) vs log AC frequency considering measured medium conductivity of the particle solution (Figure S2c). Figure demonstrating time-lapse sequence of 20 nm particle trapping (Figure S3). Figure Showing the electrothermal flow around a single fiber for both low and high-frequency cases (Figure S4). Real time movie of DEP attraction/repulsion of 1 µm particles with an applied electric potential of 7 V_{rms} and a range of frequencies, spanning from 1 kHz to 1 MHz (Supplementary Information Movie).

Author Contributions

Tonoy K. Mondal: Conceptualization, Methodology, Investigation, Validation, Software, Formal Analysis, Data Curation, Visualization, Writing- Original Draft. **Jacob H. West:** Methodology, Investigation, Visualization. **Stuart J. Williams:** Conceptualization, Validation, Funding acquisition, Resources, Project administration, Supervision, Writing-Review & Editing.

Conflicts of interest

There are no conflicts to declare.

Acknowledgement

This research work was supported by National Science Foundation under award no. 2121008. We would also like to thank the engineers in the Micro/ Nano Technology Center at the University of Louisville for the sample-specific direction for imaging under the electron microscope.

References

1. G. M. Whitesides and B. Grzybowski, *Science*, 2002, **295**, 2418-2421.

2. Y. Hwang, H. Sohn, A. Phan, O. M. Yaghi and R. N. Candler, *Nano Letters*, 2013, **13**, 5271-5276.
3. E. Babaei, D. Wright and R. Gordon, *Nano Letters*, 2023, **23**, 2877-2882.
4. D. Braun and A. Libchaber, *Physical review letters*, 2002, **89**, 188103.
5. M. Krishnan, N. Mojarad, P. Kukura and V. Sandoghdar, *Nature*, 2010, **467**, 692-695.
6. J. Han, F. Niroui, J. H. Lang and V. Bulović, *Nano Letters*, 2022, **22**, 8258-8265.
7. C. T. Ertsgaard, N. J. Wittenberg, D. J. Klemme, A. Barik, W.-C. Shih and S.-H. Oh, *Nano Letters*, 2018, **18**, 5946-5953.
8. A. Barik, L. M. Otto, D. Yoo, J. Jose, T. W. Johnson and S.-H. Oh, *Nano Letters*, 2014, **14**, 2006-2012.
9. J. A. Liddle and G. M. Gallatin, *ACS Nano*, 2016, **10**, 2995-3014.
10. P. Rai-Choudhury, *Handbook of microlithography, micromachining, and microfabrication: microlithography*, SPIE press, 1997.
11. T. Subbiah, G. S. Bhat, R. W. Tock, S. Parameswaran and S. S. Ramkumar, *Journal of applied polymer science*, 2005, **96**, 557-569.
12. Y.-E. Miao and T. Liu, in *Electrospinning: Nanofabrication and Applications*, eds. B. Ding, X. Wang and J. Yu, William Andrew Publishing, 2019, DOI: https://doi.org/10.1016/B978-0-323-51270-1.00021-2, pp. 641-669.
13. A. Greiner and J. H. Wendorff, *Angewandte Chemie International Edition*, 2007, **46**, 5670-5703.
14. N. Bhardwaj and S. C. Kundu, *Biotechnology Advances*, 2010, **28**, 325-347.
15. S.-H. Kim, D. Kim and S. Lee, *Current Applied Physics*, 2006, **6**, 766-771.
16. X. Wang, C. Drew, S.-H. Lee, K. J. Senecal, J. Kumar and L. A. Samuelson, *Nano letters*, 2002, **2**, 1273-1275.
17. N. Takami, A. Satoh, M. Hara and T. Ohsaki, *Journal of the Electrochemical Society*, 1995, **142**, 2564.
18. T. Wang, Z. Chen, W. Gong, F. Xu, X. Song, X. He and M. Fan, *ACS Omega*, 2023, **8**, 22316-22330.
19. P. Joshi, L. Zhang, Q. Chen, D. Galipeau, H. Fong and Q. Qiao, *ACS Applied Materials & Interfaces*, 2010, **2**, 3572-3577.
20. S. N. Arshad, M. Naraghi and I. Chasiotis, *Carbon*, 2011, **49**, 1710-1719.

21. F. J. García-Mateos, R. Ruiz-Rosas, J. M. Rosas, J. Rodríguez-Mirasol and T. Cordero, *Frontiers in Materials*, 2019, **6**, 114.
22. J. S. Im, S. J. Kim, P. H. Kang and Y.-S. Lee, *Journal of Industrial and Engineering Chemistry*, 2009, **15**, 699-702.
23. J. J. Ge, H. Hou, Q. Li, M. J. Graham, A. Greiner, D. H. Reneker, F. W. Harris and S. Z. Cheng, *Journal of the American Chemical Society*, 2004, **126**, 15754-15761.
24. G. Otieno and J.-Y. Kim, *Journal of Industrial and Engineering Chemistry*, 2008, **14**, 187-193.
25. H. Yui, G. Wu, H. Sano, M. Sumita and K. Kino, *Polymer*, 2006, **47**, 3599-3608.
26. K. T. Peter, J. D. Vargo, T. P. Rupasinghe, A. De Jesus, A. V. Tivanski, E. A. Sander, N. V. Myung and D. M. Cwiertny, *ACS applied materials & interfaces*, 2016, **8**, 11431-11440.
27. S. D. McCullen, D. R. Stevens, W. A. Roberts, S. S. Ojha, L. I. Clarke and R. E. Gorga, *Macromolecules*, 2007, **40**, 997-1003.
28. E. J. Ra, K. H. An, K. K. Kim, S. Y. Jeong and Y. H. Lee, *Chemical Physics Letters*, 2005, **413**, 188-193.
29. P. Heikkilä and A. Harlin, *Express Polymer Letters*, 2009, **3**, 437-445.
30. R. S. Barhate and S. Ramakrishna, *Journal of Membrane Science*, 2007, **296**, 1-8.
31. H. A. Pohl, *The behabior of neutral matter in nonuniform electric fields*, 1978.
32. R. Pethig, *Biomicrofluidics*, 2010, **4**.
33. N. R. Wood, A. I. Wolsiefer, R. W. Cohn and S. J. Williams, *Electrophoresis*, 2013, **34**, 1922-1930.
34. R. Krupke, F. Hennrich, H. v. Löhneysen and M. M. Kappes, *Science*, 2003, **301**, 344-347.
35. D. Cheon, S. Kumar and G.-H. Kim, *Applied Physics Letters*, 2010, **96**.
36. J. Kim, S. Lee, J.-K. Francis Suh, J. Ho Park and H.-J. Shin, *Applied Physics Letters*, 2013, **102**.
37. L. Novotny, R. X. Bian and X. S. Xie, *Physical Review Letters*, 1997, **79**, 645.
38. R. Krupke, F. Hennrich, M. M. Kappes and H. v. Löhneysen, *Nano Letters*, 2004, **4**, 1395-1399.
39. L. Zheng, S. Li, J. P. Brody and P. J. Burke, *Langmuir*, 2004, **20**, 8612-8619.

40. S. Tuukkanen, J. J. Toppari, A. Kuzyk, L. Hirviniemi, V. P. Hytönen, T. Ihalainen and P. Törmä, *Nano Letters*, 2006, **6**, 1339-1343.
41. F. R. Madiyar, L. U. Syed, C. T. Culbertson and J. Li, *ELECTROPHORESIS*, 2013, **34**.
42. P. U. Arumugam, H. Chen, A. M. Cassell and J. Li, *The Journal of Physical Chemistry A*, 2007, **111**, 12772-12777.
43. M. Farasat, S. M. Chavoshi, A. Bakhshi, A. Valipour and M. Badieirostami, *Journal of Micromechanics and Microengineering*, 2022, **32**, 015008.
44. Y.-K. Cho, S. Kim, K. Lee, C. Park, J.-G. Lee and C. Ko, *ELECTROPHORESIS*, 2009, **30**, 3153-3159.
45. M. Lorenz, D. Malangré, F. Du, M. Baune, J. Thöming and G. R. Pesch, *Analytical and bioanalytical chemistry*, 2020, **412**, 3903-3914.
46. H. Morgan and N. G. Green, *AC electrokinetics: colloids and nanoparticles*, Research Studies Press, 2003.
47. H. Morgan, M. P. Hughes and N. G. Green, *Biophysical journal*, 1999, **77**, 516-525.
48. A. Castellanos, A. Ramos, A. Gonzalez, N. G. Green and H. Morgan, *Journal of Physics D: Applied Physics*, 2003, **36**, 2584.
49. A. Ramos, H. Morgan, N. G. Green and A. Castellanos, *Journal of Physics D: Applied Physics*, 1998, **31**, 2338.
50. T. M. Squires, *Lab on a Chip*, 2009, **9**, 2477-2483.
51. A. Ramos, H. Morgan, N. G. Green and A. Castellanos, *Journal of Colloid and Interface Science*, 1999, **217**, 420-422.
52. R. Hölzel and R. Pethig, *Electrophoresis*, 2021, **42**, 513-538.
53. Y. Li, Y. Wang, K. Wan, M. Wu, L. Guo, X. Liu and G. Wei, *Nanoscale*, 2021, **13**, 4330-4358.